DOI:
10.1063/1.5089959

Document Version
Peer reviewed version

Double-pulse characterization by Self-Referenced Spectral Interferometry

L. Gulyás Oldal [†)],[1,*)] T. Csizmadia,[1,†)] P. Ye,[1] N. G. Harshitha,[1] M. Füle,[1] and A. Zaïr[1,2]
[1)] *ELI-ALPS, ELI-HU Non-Profit Ltd., H-6720 Szeged, Hungary*
[2)] *King's College, Department of Physics, WC2R 2LS London, United Kingdom*

(Dated: 10 July 2019)

The reconstruction of ultrashort optical pulses with complex intensity substructure is demonstrated using the Self-Referenced Spectral Interferometry (SRSI) pulse characterization technique with a modified phase retrieval algorithm. A correction spectral phase term is extracted by the manipulation of the temporal interferogram allowing the treatment of scenarios with complicated pulse shapes, where the original algorithm fails. The improved SRSI algorithm is verified through the application on two temporally well-separated pulses having the same polarization direction and spectral shape, generated by duplicating 37 fs-long amplified pulses of a Ti:Sa based laser system. The spectral phase of highly chirped double pulses with equal or different amplitude ratios is numerically retrieved. The collinear and achromatic experimental arrangement results in a compact and easy-to-align system.

PACS numbers: Valid PACS appear here

Few-cycle laser pulses have already been generated by several research groups[1–3] allowing the study of ultrafast processes in atoms and molecules[4–6] and also control chemical reactions[7]. However, the outcome of these processes due to their nonlinear nature, strongly depends on the temporal profile of the applied laser pulses. Therefore, the complete (amplitude and phase) temporal characterization of laser pulses is of utmost importance, which has led to the development of dissimilar pulse characterization techniques[8–12].

Nowadays, the Self-Referenced Spectral Interferometry (SRSI)[13] is a popular method for determining the time evolution of ultrashort optical pulses. It is based on the interference of an unknown pulse and a self-created reference pulse, which is generated by a third-order nonlinear optical effect[14]. This frequency conserved nonlinear process can be cross-polarized wave (XPW) generation[12,15], self-diffraction (SD)[16,17] or transient-grating (TG) signal production[18,19] resulting in an achromatic arrangement. The alignment can also be implemented in a collinear way making the SRSI setup simple, easily adjustable and compact in comparison with other well known characterization techniques, such as Frequency-Resolved Optical Gating (FROG)[9] and Spectral Phase Interferometry for Direct Electric-field Reconstruction (SPIDER)[10]. Also preliminarily assumptions regarding the temporal pulse shape are not needed within the phase retrieval algorithm as is required by the FROG technique.

The SRSI pulse characterization method is based on the measurement of the interference between the reference pulse and the delayed unknown laser pulse. An inverse Fourier transform on the measured spectral interferogram results in three well-separated peaks in the time domain. The spectral amplitudes of both the original and the reference pulses can be analytically reconstructed by the numerical filtering the direct (DC) and alternating (AC) terms and subsequent transformation back to the frequency domain. The spectral phase is retrieved separately by the Gershberg-Saxton iterative algorithm[20].

However, the original SRSI algorithm fails to reconstruct pulses that has significant intensity substructure. One such example is double pulses with two well-separated temporal peaks, which is represented by distinct frequency bunches in the spectral domain[21]. Their spectral distance is determined by the temporal separation of the pulses and the corresponding spectral phase is equivocal. This kind of temporal double-pulse structure is usually used to generate high harmonics using a plasma mirror[22] or realizing ultrafast pump-probe experiments[23]. Most pulse characterization methods are challenged by such complicated pulse structure, however a few techniques have already been developed, such as the improved FROG algorithm[24] or the VAMPIRE technique[25] to overcome the above mentioned relative phase ambiguities[26].

This letter presents a method, which allows the reconstruction of complex intensity substructures based on the experimentally advantageous SRSI technique. This improved SRSI algorithm overcomes the issue of the aforementioned phase ambiguity. We elucidate the introduced modification in the spectral phase and the theoretical calculations are compared and contrasted with experimentally performed measurements.

Figure 1 shows the experimental arrangement. The spectral interferograms were recorded using a commercial pulse characterization equipment based on the XPW-SRSI (WIZZLER, Fastlite Ultrafast Scientific Instrumentation) (gray boxed section in Figure 1). A temporal double-pulse is generated from an ultrashort laser pulse by using a sequence of a broadband polarizer (P1), a birefringent β-Barium-Borate (BBO) crystal and another

[*)] Electronic email: lenard.gulyas@eli-alps.hu
[†)] Both authors contributed equally

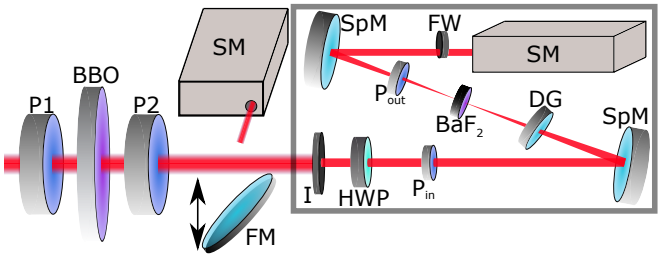

FIG. 1. (Color online) Schematic of the experimental setup: (P1, P2) polarizers, (BBO) β-Barium Borate crystal, (FM) flip mirror, (SM) broadband spectrometer. The Wizzler device, used to record the spectral interferograms, consists of an iris (I), a half-wave plate (HWP), two spherical mirrors (SpM), a delay generator (DG), a BaF_2 nonlinear crystal, input and output polarizers (P_{in}, P_{out}) and a filter wheel (FW).

broadband polarizer (P2). The first polarizer transmitted a linearly polarized beam towards the BBO crystal that split it to two orthogonally polarized pulses, the ordinary and the extraordinary ones, with τ time delay between them. τ depends on the thickness and the refractive indices of the birefringent material. The amplitude ratio of the generated pulses finely tunable by rotating the crystal. A flip mirror (FM) was inserted into the beam in order to record the spectra on a broadband VIS-IR spectrometer (Ocean Optics HR4000, SM) before the beam going into the SRSI device.

The proposed modification of the original SRSI algorithm involves the modulation of the inverse-Fourier transformed spectral interferogram (Figure 2.a red). The measured interferogram can be described as $\tilde{S}(\omega) = \tilde{S}_0(\omega) + \tilde{f}(\omega)e^{i\omega\tau_d} + c.c.$, where $\tilde{S}_0(\omega)$ is the DC and $\tilde{f}(\omega)$ is the AC term of the spectral interferogram and τ_d is the delay between them[27]. In case of a double-pulse form, the temporal AC and DC components can be written as

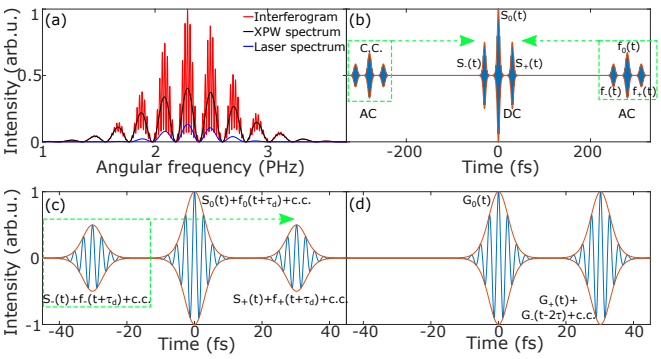

FIG. 2. (Color online) Steps to calculate the numerical spectrum to extract the correction term of the retrieved spectral phase. (a) Interferogram (red) with the XPW (black) and the laser spectrum (blue). (b) Shifting of the AC terms to overlap with the DC term. (c) Moving of the negative peak to overlap with the positive one. (d) Temporal shape of the modified Fourier-transformed spectral interferogram.

$$\tilde{f}(t) = \sum_{k=0,+,-} f_k(t) + c.c., \qquad \tilde{S}_0(t) = \sum_{k=0,+,-} S_k(t), \quad (1)$$

(Figure 2.b). The temporal separation between the consecutive $f_k(t)$ terms (or the $S_k(t)$ terms) represents the temporal separation of the double pulses, while the amplitude ratio can be extracted by simple numerical modifications using these terms. The first step of this procedure involves shifting the positive AC terms and their complex conjugates to the position of the DC term and adding them together (Figure 2 b), therefore an alternated temporal interferogram $G_k(t) = S_k(t) + f_k(t + \tau_d) + c.c.$ can be calculated (Figure 2.c). The peak $G_-(t)$ is then moved in time to overlap with the corresponding positive peak $G_+(t)$ and summarized (Figure 2.d): $S_{mod}(t) = G_0(t) + G_+(t) + G_-(t - 2\tau)$.

Applying the Fourier transform on the resulted $S_{mod}(t)$ interferogram, the spectral phase with edgy and precipitous jumps (φ_{corr}) can be extracted without higher-order dispersions. The higher-order terms (φ_{iter}) are obtained

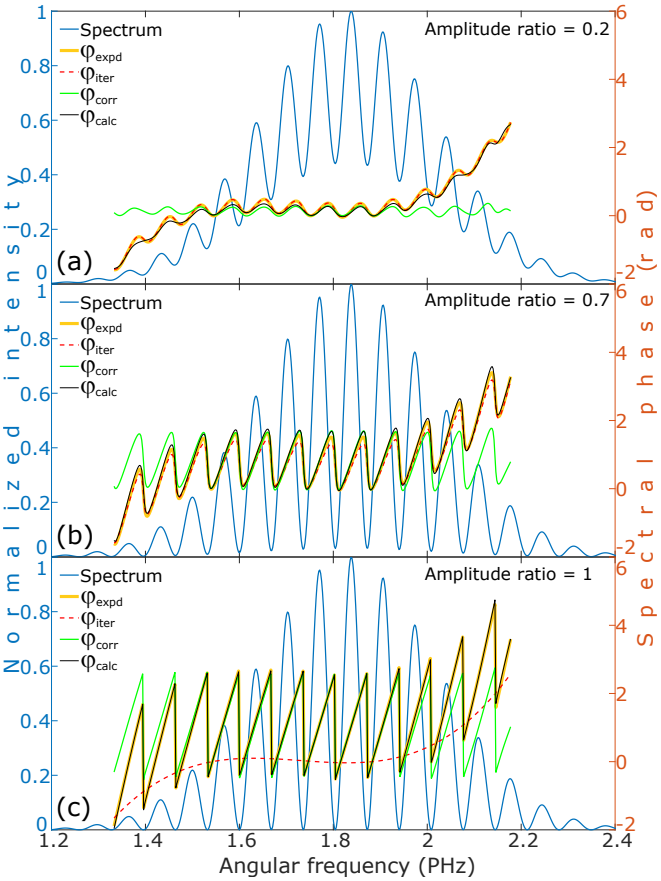

FIG. 3. (Color online) Spectra (solid blue) and the expected spectral phase (solid yellow), the outcome of the Gerchberg-Saxton iterative algorithm (red dashed), the phase correction term (solid green) and the retrieved spectral phase of double pulses at 0.2 (a), 0.7 (b) and 1 (c) amplitude ratios applying the improved algorithm (solid black).

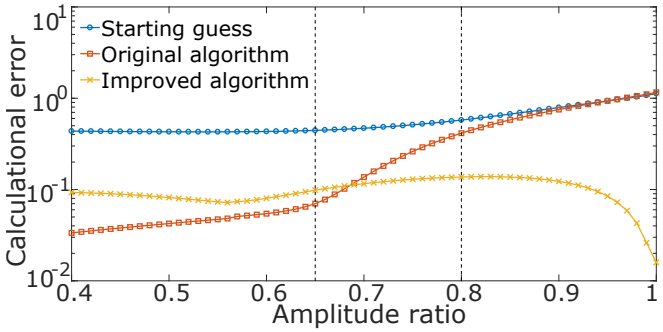

FIG. 4. (Color online) Deviation from the expected result. Blue curve with circles shows the error of the initial step of the iterative algorithm. The error of the original and the improved algorithms are shown by the orange curve with squares and the yellow curve with crosses, respectively. Parameters used in the calculation: laser central wavelength 1030 nm, pulse duration 6.2 fs, time delay 92 fs, group delay dispersion (GDD) 20 fs^2, third-order dispersion (TOD) 200 fs^3.

using the Gerchberg-Saxton iteration algorithm[20,27] assuming that the two composing pulses have the same phase (not including the CEP). The final phase (φ_{calc}) is produced by adding the two spectral phase terms together: $\varphi_{calc} = \varphi_{iter} + \varphi_{corr}$. To get better insight into the behaviour of the different algorithms, Figure 3 shows the simulated double-pulse spectrum and four phase terms at different amplitude ratios: the output phase of the original Gerchberg-Saxton algorithm (φ_{iter} - dashed red), the output phase of the improved algorithm (φ_{calc} - solid black), the correction term of the improved algorithm (φ_{corr} - solid green) and the phase to be retrieved (φ_{expd} - solid yellow). For temporal double-pulse, as their amplitude ratio is more and more comparable (Figure 3.a-c), the spectral valleys deepen in the spectrum, and edgy and precipitous jumps appear more prevalently in the spectral phase. As shown by the dashed red curve, the original algorithm can retrieve only continuous phase curves. Therefore the original method cannot retrieve this kind of phase, however the tendency of the curve inherits the dispersion terms, which can still be properly reconstructed by using the original method. Essentially, φ_{corr} contains the pulse separation and the amplitude ratio property of the double pulses and φ_{iter} provides information about the dispersion terms. By shifting the AC terms to the position of the DC term and summing them together, the effect of the delay generator in the SRSI method can be eliminated. Thereby, the XPW effect also disappears, thus the remained signal contains information only about Fourier-limited pulses.

The error of the methods can be determined by the $(\omega_2-\omega_1)^{-1}\int_{\omega_1}^{\omega_2}|\varphi_{ret}(\omega)-\varphi_{expd}(\omega)|d\omega$ formula, where the expected and retrieved phase are defined as $\varphi_{expd}(\omega)$ and $\varphi_{ret}(\omega)$, respectively. The expected phase is arbitrarily defined. The deviation of the outcome of original and upgraded techniques from the input phase is presented as a function of the amplitude ratio of the two temporal peak in Figure 4. The blue curve with circles shows the initial guess of the iterative algorithm and the error of the original (orange curve with squares) and the improved (yellow curve with crosses) algorithm are presented as well. This figure shows that the original algorithm is inaccurate when the amplitude ratio is greater than 0.65 and it does not deviate significantly from the initial estimate for an amplitude ratio grater than 0.8. By making the modification in the retrieved phase, at the high amplitude ratios, the improved algorithm provides results with substantially smaller error than the original one. Below amplitude ratio 0.7 the error of the improved method is higher than the fundamental technique but still less than 10%, which shows the competency of the developed method to adequately reconstruct double pulses at any arbitrary amplitude ratios.

Spectral interferograms were recorded from an arbitrary 0° to 90° of the BBO in 5° steps adjusted by a manually rotatable stage. The temporal amplitude, after the second polarizer ($P2$) of the ordinary ($A_o = A \cdot cos^2\alpha$) and the extraordinary ($A_e = A \cdot sin^2\alpha$) pulses can be calculated using simple geometric considerations. From these expressions, the angle-dependent temporal amplitude ratio of the pulses can be expressed as:

$$\frac{A_e}{A_o} = \frac{A \cdot sin^2\alpha}{A \cdot cos^2\alpha} = tan^2\alpha, \qquad (2)$$

where α is the angle between the axis of the BBO crystal ($\overline{o}$) and the polarization direction of the laser beam ($\overline{I}$). The measured amplitude ratios as a function of the calibrated rotational angles are presented in Figure 5 (orange dots). A $tan^2(\alpha+\delta)$ function was fitted (blue curve) on the measured data, where δ was the offset parameter, with which the arbitrary angles of the crystal rotation were subsequently validated. Nevertheless, this technique cannot distinguish the ordinary and the extraordinary pulses, thus the maximal amplitude ratio is

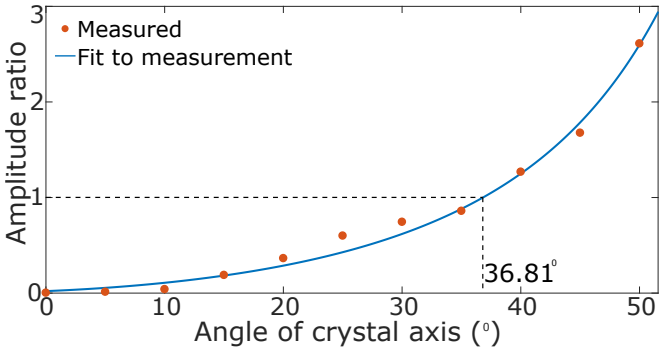

FIG. 5. (Color online) Measured amplitude ratios (orange dots) of the reconstructed double pulses, calculated by the improved algorithm. The blue line represents the $\tan^2(\alpha+\delta)$ fitting to the experimentally measured amplitude ratios. The indicated value shows the crystal angle, where the pulses are generated with equal amplitude.

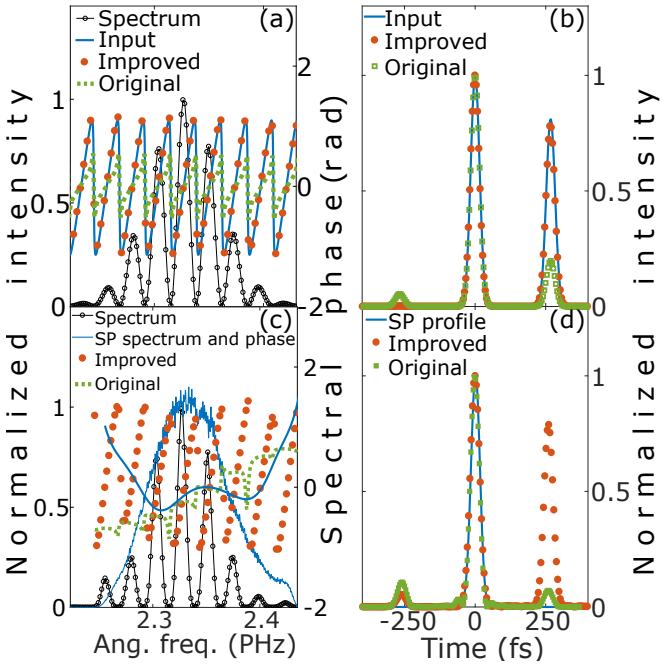

FIG. 6. (Color online) (a) Spectrum of the simulated double pulses (black line with open circles), the corresponding spectral phase (solid blue) and its retrieval with the improved (orange dots) and with the original (green dotted line) algorithm. (b) The simulated double-pulse (solid blue) and the result of the reconstruction applying the improved (orange dots) and the original (green squares) method. (c) Spectrum of single-pulse (SP) and the corresponding spectral phase extracted from the WIZZLER apparatus (solid blue), the measured spectral amplitude of double pulses (black line with open circles), the retrieved phase with our algorithm (orange dots) and the outcome of the SRSI device (green dotted line). (d) The corresponding SP shape (solid blue) and double-pulse shapes reconstructed by our algorithm (orange dots) and the result of the SRSI device (green squares).

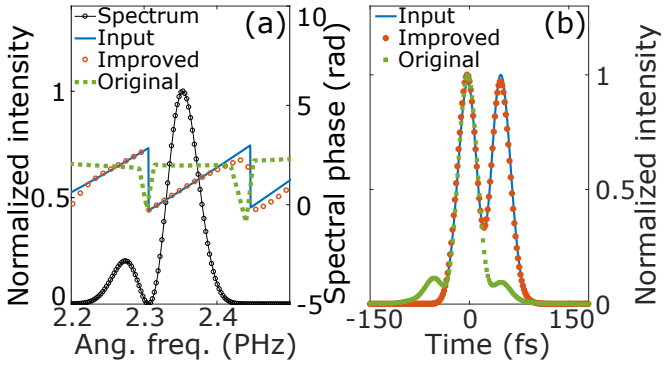

FIG. 7. (Color online) Reconstruction of temporally overlapped pulses. Figure (a) shows the spectrum (black line with open circles), the input (solid blue) phase and its reconstruction with the original (green squares) and improved (red open circles) algorithm. The corresponding temporal profiles are presented by figure (b). The pulse duration is 37 fs and the delay between them is 45 fs.

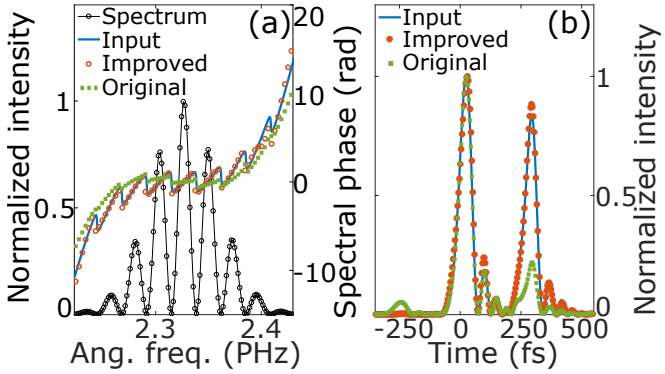

FIG. 8. (Color online) Temporal profile ((b), solid blue) and the spectral amplitude ((a), black line with open circles) of the simulated double pulses. Simulated spectral phase ((a), solid blue) and its retrieval by the original ((a), green squares) and the improved method ((a), orange open circles) introducing higher-order dispersion. The reconstruction of the temporal shape by the original and the improved algorithm is presented by the green squares and the orange dots in figure (b), respectively.

1 and after this amplitude ratio the reciprocal value was calculated in Figure 5. The information about the correct sequence of pulses, however, can be gathered by knowing the orientation of the crystal and its direction of rotation during the record of the data.

Experimental measurements (Figure 6.c/d) and theoretical calculations (Figure 6.a/b) were compared, when the amplitude ratio was higher than 0.7. Experimental measurements were made using the pulses of a Ti:Sa laser system, which spectrum is shown by (Figure 6.c, solid blue), with a transform limited duration of 37 fs (Figure 6.d, solid blue). The double pulses were generated using a 700 μm thick BBO crystal to introduce $\sim$268 fs delay between the divided ordinary and the extraordinary pulses. Simulations used a 37 fs length, Gaussian shape pulse and its delayed replica with 90% amplitude of the original (Figure 6.b solid blue) with a delay of 268 fs. The spectral amplitude with the valleys (Figure 6.a black line with open circles) and the corresponding complex spectral phase (Figure 6.a solid blue) were numerically calculated by applying the Fourier-transform. Higher-order dispersions have not been added to this spectral phase. The results of the phase retrieving using the improved (orange dots) and the original (green dotted line) algorithm are presented in the Figure 6.a and the related temporal pulse shapes are visible in the Figure 6.b (orange dots and green squares, respectively). The pulse reconstruction from the experimental spectral interferogram is shown in Figure 6.c/d. The black curve with open circles shows the recorded spectrum, the retrieved phase and the reconstructed pulse shape applying the improved algorithm are represented by the orange circles. In Figure 6.c, the green dotted phase curve was extracted from the SRSI device and the corresponding pulse shape are plotted with green squares in Figure 6.d.

The above results prove the pertinence of the improved algorithm when the pulses are completely separated or their temporal amplitude is different. Nevertheless, the time delay between them is also a key parameter. At short time delays, the density of the frequency component bunches in the spectrum is decreased. Both the original and the improved algorithm provide incorrect result, if there appear only two spectral bunches and one of them is not intense enough. However, in case of clearly distinguishable spectral bunches, the improved algorithm gives correct outcome, but the original algorithm still inaccurate. The result of the reconstruction of partially overlapped pulses is presented in Figure 7.

A final inspection of the techniques was the simulation of adding group delay dispersion (GDD) and third-order dispersion (TOD) to the spectral phase, $300 fs^2$ and $60000 fs^3$ were set, respectively. The other parameters of the simulation were the same as Figure 6.a/b. Figure 8 shows that the reconstruction of the simulated highly chirped temporal pulse shape matched the original shape well. The high TOD resulted several low satellites in the temporal profile but the algorithm could reconstruct the double pulses. In general, similarly to the original SRSI algorithm[27], the validity of the reconstruction can be checked by the determination of a broadening coefficient (Z) defined by the ratio of the XPW and the input pulse spectral widths ($Z = \omega_{XPW}/\omega_0$). As a rule of thumb, the measurement is valid as long as $Z > Z_{limit}$, where $Z_{limit} = 1$ for Gaussian, and $Z_{limit} > 1$ for super-Gaussian composing pulse forms. It is important to note, that even with GDD values slightly bigger than the values determined by the broadening criterion, the phase can possibly be recovered, however the user will not be able to assure the validity of phase retrieval process in this case.

In conclusion, an upgraded spectral phase retrieval algorithm was demonstrated to improve the SRSI pulse characterization method. The extraction of a correction term of the spectral phase from the manipulated Fourier-transformed spectral interferogram enables the characterization of temporal double pulses having the same spectral amplitude whilst maintaining the ability to reconstruct simpler spectral shapes. Temporal double pulses is common in laser physics, however it is not the only pulse form having elaborate intensity behaviour that can occur. The reconstruction of this representative case of a complex temporal shape, shows that the improved SRSI algorithm in general opens up the possibility to reconstruct the temporal envelopes of pulses with arbitrary intensity substructure and thus enabling better characterization and application of ultrashort light pulses.

We are grateful for the help of Roland Flender and János Csontos at the TeWaTi laboratory of the University of Szeged. This work was financially funded by the ELI-ALPS project (GINOP-2.3.6-15-2015-00001), which is supported by the European Union and co-financed by the European Regional Development Fund. We also acknowledge funding from the Ministry of Human Capacities of Hungary under the Grant "National Programme of Talents", application no. NTP-NFTÖ-18-B-0088.

[1] R. Budriūnas, T. Stanislauskas, A. Aleknavičius, J. Adamonis, G. Veitas, D. Gadonas, S. Balickas, A. Michailovas, and A. Varanavičius, Optics Express **25**, 5797 (2017).
[2] S. Hädrich, M. Kienel, M. Müller, A. Klenke, J. Rothhardt, R. Klas, T. Gottschall, T. Eidam, A. Drozdy, Z. Várallyay, et al., Optics Letters **41**, 4332 (2016).
[3] N. Thiré, R. Maksimenka, B. Kiss, C. Ferchaud, P. Bizouard, E. Cormier, K. Osvay, and N. Forget, Optics Express **25**, 1505 (2017).
[4] T. Zuo, A. D. Bandrauk, and P. B. Corkum, Chemical Physics Letters **259**, 313 (1996).
[5] H. C. Shao and A. F. Starace, Physical Review Letters **105**, 263201 4pp (2010).
[6] E. Goulielmakis, Z. H. Loh, A. Wirth, R. Santra, M. F. Kling, N. Rohringer, V. S. Yakovlev, S. Zherebtsov, T. Pfeifer, A. M. Azzeer, et al., Nature **466**, 739 (2010).
[7] A. Assion, T. Baumert, M. Bergt, T. Brixner, B. Kiefer, V. Seyfried, M. Strehle, and G. Gerber, Science **282**, 919 (1998).
[8] I. D. Jung, F. X. Kärter, J. Henkmann, G. Zhang, and U. Keller, Applied Physics B **65**, 307 (1997).
[9] R. Trebino and D. J. Kane, Journal of Optical Society of America A **10**, 1101 (1993).
[10] C. Iaconis and I. A. Walmsley, Optics Letters **23**, 792 (1998).
[11] L. Gallmann, D. H. Sutter, N. Matuschek, G. Steinmeyer, and U. Keller, Applied Physics B **70**, S67 (2010).
[12] T. Oksenhendler, S. Coudreau, N. Forget, V. Crozatier, S. Grabielle, R. Herzog, O. Gobert, and D. Kaplan, Applied Physics B **99**, 7 (2010).
[13] X. Shen, P. Wang, J. Liu, T. Kobayashi, and R. Li, Applied Sciences **7**, 407 (2017).
[14] N. Minkovski, G. I. Petrov, , S. M. Saltiel, O. Albert, and J. Etchepare, Journal of the Optical Society of America B **21**, 1659 (2004).
[15] A. Jullien, L. Canova, O. Albert, D. Boschetto, L. Antonucci, Y. H. Cha, J. P. Rousseau, P. Chaudet, G. Chériaux, J. Etchepare, et al., Applied Physics B **87**, 595 (2007).
[16] J. Liu, K. Okamura, Y. Kida, and T. Kobayashi, Optics Express **18**, 22245 (2010).
[17] J. Liu, Y. Jiang, T. Kobayashi, R. Li, and Z. Xu, Journal of the Optical Society of America B **29**, 29 (2012).
[18] J. Liu, K. Okamura, Y. Kida, and T. Kobayashi, Chinese Optics Letters **9**, 051903 3pp (2011).
[19] J. Liu, F. J. Li, Y. L. Jiang, C. Li, Y. X. Leng, T. Kobayashi, R. X. Li, and Z. Z. Xu, Optics Letters **37**, 4829 (2012).
[20] R. W. Gerchberg and W. O. Saxton, Optik **35**, 237 (1972).
[21] R. Paschotta, Encyclopedia of laser physics and technology **1**, 856pp (2008).
[22] C. Thaury, F. Quéré, J.-P. G. A. Levy, T. Ceccotti, P. Monot, M. Bougeard, F. Réau, P. D'oliveira, P. Audebert, R. Marjoribanks, et al., Nature Physics **3**, 424 (2007).
[23] A. Assion, M. Geisler, J. Helbing, V. Seyfried, and T. Baumert, Applied Physics B **54**, R4605 4pp (1996).
[24] K. W. DeLong and R. Trebino, Journal of Optical Society of America A **11**, 2429 (1994).
[25] B. Seifert and H. Stolz, Measurement Science and Technology **20**, 015303 7pp (2009).
[26] D. Keusters, H.-S. Tan, P. O'Shea, E. Zeek, R. Trebino, and W. S. Warren, Journal of the Optical Society of America B **20**, 2226 (2003).
[27] T. Oksenhendler, arXiv:1204.4949 p. 37 pp (2012).